Published in final edited form as:

Biomaterials. 2014 June ; 35(19): 5098–5109. doi:10.1016/j.biomaterials.2014.03.011.

Carbon nanotube-based substrates for modulation of human pluripotent stem cell fate

Marina V. Pryzhkova[a], **Indrat Aria**[b], **Qingsu Cheng**[c], **Greg M. Harris**[a], **Xingjie Zan**[d], **Morteza Gharib**[b], and **Ehsan Jabbarzadeh**[a,c,e,*]

[a] Department of Chemical Engineering, University of South Carolina, SC 29208, USA

[b] Graduate Aeronautics Laboratories, California Institute of Technology, CA 91125, USA

[c] Department of Biomedical Engineering, University of South Carolina, SC 29208, USA

[d] Department of Chemistry and Biochemistry, University of South Carolina, SC 29208, USA

[e] Department of Orthopaedic Surgery, University of South Carolina, SC 29208, USA

Abstract

We investigated the biological response of human pluripotent stem cells (hPSCs) cultured on a carbon nanotube (CNT) array-based substrate with the long term goal to direct hPSC germ layer specification for a wide variety of tissue engineering applications. CNT arrays were fabricated using a chemical vapor deposition system allowing for control over surface roughness and mechanical stiffness. Our results demonstrated that hPSCs readily attach to hydrophilized and extracellular matrix coated CNT arrays. hPSCs cultured as colonies in conditions supporting self-renewal demonstrated the morphology and marker expression of undifferentiated hPSCs. Conditions inducing spontaneous differentiation lead to hPSC commitment to all three embryonic germ layers as assessed by immunostaining and RT-PCR analysis. Strikingly, the physical characteristics of CNT arrays favored mesodermal specification of hPSCs. This is contradictory to the behavior of hPSCs on traditional tissue culture plastic which promotes the development of ectoderm. Altogether, these results demonstrate the potential of CNT arrays to be used in the generation of new platforms that allow for precise control of hPSC differentiation by tuning the characteristics of their physical microenvironment.

Keywords

Multi-walled carbon nanotubes; Surface roughness; Human pluripotent stem cells; Differentiation; Cell adhesion; Cytoskeleton

1. Introduction

Human pluripotent stem cells (hPSCs) possess unique capabilities of almost indefinite self-renewal and proliferation as well as the ability to produce all human cell types under the

* Corresponding author. University of South Carolina, Columbia, SC 29208, USA. Tel.: +1 (803) 777 3297; fax: +1 (803) 777 8265. jabbarza@cec.sc.edu, ehsan@sc.edu (E. Jabbarzadeh).

appropriate conditions. These exceptional characteristics make hPSCs an attractive option for regenerative medicine and tissue engineering. Human embryonic stem cells (hESCs) are pluripotent cells that can differentiate into derivatives of all three embryonic germ layers both *in vitro* and *in vivo* [1,2]. Another promising source of hPSCs under investigation includes induced pluripotent stem cells (iPSCs) [3–5].

Currently, a number of research groups are working on the development of efficient differentiation protocols for the generation of complete, functional tissue comprised of hPSC derivatives through two-dimensional *in vitro* culture or three-dimensional embryoid body approaches [6]. However, traditional *in vitro* culture is a poor choice to mimic all microenvironmental factors which cooperate to direct stem cell differentiation in a developing organism [6]. A few of these key factors include the surrounding microenvironmental structure including surface topography and roughness, extracellular matrix (ECM) elasticity, ECM proteins, cellecell interactions, and other physical forces affecting the cell. These microenvironmental forces combined with chemical factors work together to control cellular differentiation and behavior [7,8]. A recent pioneering study was able to show that simply controlling cell size with 20 μm^2 and 75 μm^2 diameter fibronectin covered islands can promote cell apoptosis or growth respectively [9]. Substrate elasticity is also a potent regulator of cell behavior with studies showing that ECM elasticities of 1 kPa, 8 kPa, and 25 kPa upregulate expression of neurogenic, myogenic, and osteogenic markers in human mesenchymal stem cells respectively [10]. Engineered 3D scaffolds with differing elasticities have also been successfully employed to direct hESC differentiation into specific germ layers [11]. ECM topography is another key factor in the modulation of the cytoskeletal organization and cell migration [12]. Cells are able to respond to surface nanotopography by altering cell morphology and alignment corresponding to nanoscale substrate features [13–15].

Because of their size and tunable chemical properties, CNTs offer a wide range of therapeutic applications including gene alterations, drug delivery, and medical diagnosis [16–20]. CNT-based platforms offer the unique opportunity to combine several microenvironmental factors to cooperatively direct hPSC differentiation. CNTs have the potential to tune surface properties and attain differing degrees of CNT wettability and specific ligand attachment sites [11,21]. CNTs also are able to provide outstanding thermal and electrical conductivity as an avenue for further control of hPSC fate [22,23]. However, there is a profound need to characterize the individual effects of CNTs on hPSC behavior. To date, very few studies have characterized hPSCs and the early steps of germ layer commitment in relation to materials blended with CNTs. In one of these studies, it was reported that a higher yield of nestin positive cells was obtained through hESCs that spontaneously differentiated on collagen/CNT composites than on collagen alone [24]. It was also shown that mouse iPSCs possess increased cell adhesion, decreased colony spreading, and form hemiround colonies [25]. Although these studies implicate CNTs as a potential contributor to cell behavior, their role in germ layer commitment has been largely unexplored.

In this study we aimed to investigate hPSC behavior on CNT arrays and their capability to attach, proliferate, and differentiate on tunable CNT arrays. To achieve this goal, we sought

to characterize the surface properties of unmodified and ozone-treated CNT arrays and provide ligand attachment sites for hPSCs. We then further investigated hPSC behavior on conditions supporting self-renewal or differentiation. The evaluation of CNT arrays capability to direct hPSC commitment into a specific embryonic germ layer was based on corresponding gene and protein expression profile of differentiated cells. These experiments further open new opportunities for cooperative mechanobiological and electrobiological studies of hPSC response to external microenvironment signals and the development of methods for their directed differentiation into tissue-specific cell types.

2. Materials and methods

2.1. Fabrication of CNT arrays

CNT arrays were fabricated by employing a chemical vapor deposition (CVD) system [26]. In brief, silicon wafers (WRS) were coated with a 1–2 nm layer of iron nanoparticles and placed in a quartz tube (2 inches in diameter). The quartz tube was then heated to 750 °C at atmosphere pressure and 750 sccm argon (Praxair, 99.99%) was purged into the tube for 5 min. A mixture of gas containing 80 sccm ethylene (Praxair, 99.99%), 50 sccm hydrogen (Praxair, 99.99%), and 750 sccm argon was lastly purged into the quartz tube to allow growth of the CNT array for 1 h.

2.2. Functionalization of CNT arrays

CNT arrays were oxidized with a UV/ozone cleaner (BioForce Nanosciences) for 5 min prior to use. The degree of wettability for the CNT arrays was analyzed with a water droplet method [21]. Oxidized CNT arrays were coated with Geltrex (Invitrogen) in a 1:400 dilution at 37 °C for 1 h followed by incubation at room temperature for 1 h.

2.3. Characterization of CNT morphology and roughness

Samples used for characterization analysis were as follows: tissue culture treated plastic 6-well plates (BD) with and without Geltrex coating, CNT arrays with and without UV/ozone treatment, and CNT arrays treated with UV/ozone and coated with Geltrex.

Morphology of the CNT arrays was characterized through scanning electron microscopy (SEM). CNT arrays were visualized without treatment while Geltrex-coated CNT arrays were prepared through freeze-drying. In short, samples were fixed in 2.5% glutaraldehyde for 4 h, excess liquid carefully removed, further immersed into liquid nitrogen, and quickly transferred to a vacuum chamber for concurrent freeze-drying and sputter coating with gold/palladium [27] (Denton Desk II). The samples were viewed with a Zeiss Ultraplus FESEM at an accelerating voltage of 5–15 kV.

Prior to AFM measurements, Geltrex-coated samples were dehydrated at room temperature. AFM images were obtained at ambient conditions using a NanoScope IIIA MultiMode AFM (Veeco) in tapping mode. A scan field of 10 × 10 μm with a scan rate of 1 Hz was used for measurements. The data was analyzed using NanoScope imaging software.

2.4. hPSC growth and differentiation

hESC line H9 was purchased from WiCell (Wisconsin)(1) and hiPSC line BM1M was kindly provided by Dr. I. Slukvin (University of Wisconsin-Madison) [5]. All cell lines were grown on a mouse embryonic fibroblast (MEF) (Millipore) feeder layer in DMEM/F12 (Invitrogen) with 20% KnockOut SR (Invitrogen), 0.1 mM MEM Non-Essential Amino Acids (Invitrogen), 3.5 mM L-Glutamine (final concentration) (Invitrogen), 0.1 mM 2-Mercaptoethanol (Sigma), and supplemented with 10 ng/ml human recombinant bFGF (PeproTech) (also see WiCell Protocols). Medium was changed daily and cells were passaged on the fifth day of culture with collagenase type IV (Invitrogen). MEF cells were grown in DMEM (Invitrogen) with 10% FBS (Invitrogen or Atlas Biologicals) and 100 U/100 μg/ml of penicillin/streptomycin (Invitrogen).

hPSC monolayer culture with single cell passaging was established as described [28]. In brief, hPSCs were switched from feeder-dependent culture to feeder-free conditions and were grown as colonies for 2–3 passages on growth factor reduced Geltrex (1:400) (Invitrogen) coated 6-well plates in MEF-conditioned medium supplemented with 10 ng/ml hrbFGF. Cells were passaged mechanically on day five of culture. Conditioned medium was prepared as described [28]. In brief, MEF cells were mitotically inactivated with Mitomycin C at 10 μg/ml for 2.5 h (Sigma) and then plated onto gelatinized flasks (Gelatin, Sigma) at a density 60,000 cells/cm^2. The following day cells were washed with phosphate buffer solution (PBS) (Sigma), medium was changed to hESC medium (without hrbFGF) at 0.5 ml/cm^2 and then collected every 24 h for 7 days. Before use conditioned medium was filtered and supplemented with 10 ng/ml hrbFGF. On the day of colony to single cell passaging hPSC colonies were treated with TrypLE Select (Invitrogen) for 1 min, gently dissociated to single cells, and plated to new wells at approximate 80–100,000 cells/cm^2. Cells were grown under identical culture conditions and single cell passaged upon reaching confluence. After stabilization of the cell culture, cells were passaged as single cells on each fourth day at a seeding density of 50,000 cells/cm^2. To study the behavior of single hPSCs on CNT arrays, 10 μM ROCK inhibitor (Y-27632, Calbiochem) was added to hPSC culture medium 2 h before cell seeding, after cell seeding overnight, or both.

Differentiation studies on CNT arrays were performed in DMEM/F12 (Invitrogen) supplemented with 15% FBS (Atlas Biologicals). hPSCs were collected as per routine passaging methods and plated on CNT arrays in 24-well plates or low attachment 6-well plates for 8 days for embryoid body formation followed by further differentiation on CNT arrays. Medium was changed each third day for these trials. Before plating cells CNT arrays were disinfected for 2–3 h in 70% ethanol (Decon Labs), ethanol was allowed to evaporate, and arrays were then washed three times with PBS. Geltrex coating of CNT arrays was performed as described: Geltrex was diluted 1:400 in cold DMEM/F12 (Invitrogen) and added into the wells of 24-well plates containing CNT arrays. Plates were incubated for 1 h at 37 °C followed by 1 h at room temperature. Geltrex solution was replaced by hPSC medium immediately before plating cells.

2.5. hPSC morphology, immunostaining, and RT-PCR

For SEM analysis of hPSC colonies on CNT arrays traditional chemical fixation and dehydration methods were used. Cells were fixed in 2.5% glutaraldehyde for 4 h before dehydrating in a series of ethanol dilutions with increasing concentration (30%, 50%, 70%, 90%, 100%) for 10 min each. Samples were allowed to dry at room temperature overnight, sputter coated with gold, and visualized by SEM.

For immunostaining cells were washed with PBS (Sigma), fixed with 10% formalin (Sigma) for 20 min, and permeabilized with 0.1% Triton-X 100 (Sigma). To prevent non-specific antibody binding cells were incubated for 30 min in blocking solution (PBS containing 4% goat serum) (Sigma). Cells were then incubated with primary antibodies in blocking solution for 1 h, washed with Rinse Buffer (Tris–HCl + 0.05% Tween-20) (Sigma), and incubated with secondary fluorochrome-conjugated antibodies. Antibodies used are provided in Table 1. In certain cases this was followed by Rhodamine Phalloidin-TRITC staining (Invitrogen). Cells on glass coverslips (Electron Microscopy Science) were mounted onto glass slides (VWR) with DAPI-containing mounting solution (Sigma). Cells on CNT arrays and in 24-well plates were covered with mounting solution for 5–10 min to allow DNA staining and filled with PBS to prevent their drying and for further storage. Samples were analyzed and images taken using either upright Nikon Eclipse 80i or inverted Nikon Eclipse Ti fluorescent microscopes with NIS-Elements imaging software.

For gene expression analysis, cell samples were washed in PBS and total RNA was extracted using a GeneJET RNA Purification Kit (Fermentas). To exclude genomic DNA contamination samples were treated with DNase I (Fermentas). RNA quantity was measured with nanoVette using a DU 730 Spectrophotometer (Beckman Coulter). First strand cDNA synthesis was carried out with 0.5 μg RNA and oligo(dT) primers as described in the RevertAid Kit protocol (Fermentas). “Reverse transcriptase minus (RT–)” and “no template” negative controls were also performed. PCR reactions were set with DreamTaq DNA Polymerase (Fermentas). For each sample 1 μl of cDNA was used as a template. Reaction conditions applied were as described: initial denaturation at 94 °C for 2 min, (denaturation 94 °C for 30 s, annealing 58 °C for 30 s, extension 72 °C for 45 s) × 30 cycles, and final extension was carried out at 72 °C for 10 min. The list of primers (Integrated DNA Technologies) is provided in Table 2. RT-PCR reactions were performed on C1000 Thermal Cycler (BioRad). Samples were run in 1.5% agarose gels containing 1 μg/ml ethidium bromide and visualized on Molecular Imager ChemiDoc XRS+ (BioRad). GeneRuler 1 kb Plus DNA Ladder (Fermentas) was used for DNA fragments sizing.

3. Results and discussion

3.1. CNT array surface properties

The CNT arrays used in this study were fabricated by CVD method using silicon wafer substrates [26]. Heights of the CNTs were approximately 40–60 μm with the diameter for each individual CNT measuring approximately 20–50 nm (Fig. 1A). Due to the graphene present, unmodified CNTs are highly hydrophobic and allow for poor cell adhesion [29]. To overcome this obstacle the hydrophobicity of CNT arrays can be altered through treatment

with UV/ozone. This process also partially damages the graphene layer while adding oxygenated functional groups (C=O, C–OH and COOH). To achieve an optimal level of functionalization, the hydrophilic CNT arrays were chosen for cell culture [21,30]. Briefly, CNTs were UV/ozone treated for 5 min to render arrays hydrophilic and allow ECM deposition and cell attachment [21]. Fig. 1D demonstrates the degree of hydrophilicity of the CNT arrays after undergoing UV/ozone exposure.

Cell attachment to specific ECM proteins is dependent on the corresponding integrin expression profile, which varies among cell types [31]. hPSCs express laminin + entactin receptor α6β1, vitronectin receptor αVβ5 and fibronectin receptor α5β1 allowing their attachment to Geltrex or Matrigel (which include laminin, collagen IV and entactin/nidogen), vitronectin, and fibronectin [32,33]. hPSC proliferation and attachment have been shown to be completely inhibited by blocking integrin chain β1 and receptor αVβ5 with specific antibodies [32]. Thus, the appropriate ECM for cell attachment is paramount to support self-renewal capabilities as well as pluripotency. When hPSCs were seeded as clumps of cells on hydrophilic CNT arrays without ECM coating, cells were unable to adhere to arrays and underwent apoptosis. An insignificant number of small colonies were observed after three days of culture without ECM (data not shown). Therefore, we coated hydrophilic CNT arrays with Geltrex and found that it supported survival and growth of hPSCs. All further studies were performed on ECM-coated CNT arrays and Fig. 1B and C shows the efficient integration of the ECM proteins onto CNT arrays.

It has been well established that microenvironmental properties such as stiffness, roughness, surface area, and topography can significantly affect cell behavior through mechanisms of physical signaling [7,8]. To understand how CNT arrays affect hPSC behavior, we sought to characterize the nanotopography, roughness, and stiffness of our CNT arrays. Fig. 1 shows the unique surface topography of the CVD generated CNT arrays. Interestingly, single CNTs were shown to be entangled together, making the CNT arrays more closely resembling an ECM network which underlies the basal laminae of the epithelium and covers the surface of muscle, adipose, and Schwann cells [34]. Next, we performed roughness measurements of the CNT arrays using an AFM (Table 3, Fig. 2) and found the nanoroughness of pristine and UV/ozone treated CNT arrays to be in the range of approximately 500 nm. ECM coating reduced this roughness by approximately 140 nm. The CNT arrays with and without ECM coating were significantly rougher than tissue culture polystyrene (TCP) coated and non-coated with ECM (roughness lies in the range of 4–24 nm in Table 3). Surface roughness in combination with topography has previously been shown to significantly affect cell behavior leading to apoptosis or stem cell differentiation [12,14,15,35]. Contractile myofibers have also been generated from hESCs on a polymer film with average wrinkle depth of about 200–300 nm [14]. hESCs have also been induced to differentiate on glass surfaces with a surface roughness of approximately 150 nm showing the capabilities of hPSCs to sense and integrate these nanorough surfaces [15].

According to previously published reports, the Young's modulus of TCP, collagen, and glass are 700 MPa, 0.6 MPa and 60 GPa, respectively [24,36]. The modulus of the CNT arrays was measured at 0.8 MPa, which approximates the reported values for a collagen matrix [36]. Cells are shown to respond to a range of modulus's ranging from 0.1 to 55 KPa in

behaviors such as proliferation, apoptosis rate, and morphology [37]. In particular, hMSCs were shown to differentiate exclusively to osteogenic lineage on rigid substrates [10]. Mouse ESCs were shown to maintain self-renewal and pluripotency on 0.6 KPa substrates but differentiated as elasticity was increased to 8 KPa [38]. These mechanotransduction pathways are able to convert biophysical signals into biochemical signals by regulating the level of gene expression and protein synthesis [38,39]. A number of studies have shown correlations between cytoskeletal regulation and Rho GTPases, in particular the RhoA signaling cascade [40]. These signaling proteins have proven to be responsible for a number of cellular behaviors including cell adhesion, cell migration, and differentiation arising from the physical signals of the microenvironment.

3.2. hPSC pluripotency and self-renewal

For this study we used hESC line H9 and bone marrow-derived hiPSC line BM1M. Cells were grown as colonies on a feeder layer of MEF cells or under feeder-free conditions on Geltrex-coated tissue culture plastic in MEF-conditioned medium. To assess the cellular behavior on CNT arrays, hPSCs were treated with collagenase IV for passaging on day 5, resuspended in small clumps, and seeded onto CNT arrays in MEF-conditioned medium. Colony morphology and expression of pluripotency-associated markers were evaluated on day 3 and day 4 of culture using SEM and immunocytochemistry.

SEM analysis showed that hPSC clumps were able to spread on CNT arrays, formed round-shaped flattened colonies and demonstrated morphology characteristic for undifferentiated hPSC colonies in regular cell culture on TCP. Fig. 3A demonstrates hPSC colonies on CNT arrays. We then evaluated the expression of transcription factor OCT4 (nuclear localization) and surface marker trans-membrane protein TRA-1-81 and found that each marker was uniformly expressed by hPSCs (Fig. 3B, C). hPSCs cultured on CNT arrays also showed behavior similar to traditional hPSC culture systems in the time period analyzed [1,5]. Both types of hPSCs formed typical round-shaped flattened colonies and expressed pluripotency-associated markers in culture conditions supporting their undifferentiated state and self-renewal.

3.3. Migration of hPSCs

The CNT arrays in our experiments were entangled forming a randomly oriented topography, as shown in Fig. 1. In previous studies the migration of cells on randomly oriented synthetic nanofibers has been shown to be limited due to the topographical features of the ECM [41]. In general, hPSC colonies cultured in differentiation medium for eight days began losing pluripotency marker expression in the middle of the colonies (Fig. 4A) while proliferating along the periphery. Cells retained intercellular contacts and colony morphology under both self-renewal and differentiation conditions and similar behavior was observed in embryoid bodies (EB) plated on CNT arrays for further differentiation. In comparison, cells grown on Geltrex-coated TCP formed cell monolayers quickly suggesting that TCP surfaces do not affect hPSC spreading and migration. Fig. 4B shows cell–cell contacts to be absent by Day 24 and that cells had migrated from colonies and began showing distinct FA at this time.

hPSCs in colonies generally are rounded and tightly packed. Thus, it is difficult to reveal distinct individual FAs. FAs are visible only in flattened cells at the colony periphery in feeder-free culture (data not shown). To further investigate hPSCs behavior on CNT arrays, we used single hPSCs grown as monolayer cultures with single cell dissociation during passaging [28]. As it was suggested from described experiments, single hPSCs from a monolayer culture underwent apoptosis within 24 h on substrates that were not coated with Geltrex. These results suggested that the early developmental stage of hPSCs is strongly dependent on integrin-based adhesion [32,33]. Unexpectedly, most single hPSCs 24 h post-seeding onto Geltrex-coated CNT arrays also underwent apoptosis. Single cells that attached to CNT arrays demonstrated blebbing and retained a rounded shape while sparse cells were able to establish cell–ecell contacts with flattened morphology (Fig. 5). In contrast, single cells on Geltrex-coated TCP were able to migrate, reestablish cell–ecell contacts, and form cellular groups with ease. These groups uniformly expressed pluripotency marker OCT4, formed FAs on the cell periphery, and had a defined cytoskeletal structure (Fig. 5).

We also performed experiments where single hPSCs from a monolayer culture were pre-treated, post-treated, and both pre and post-treated with Rho-kinase (ROCK) inhibitor. Our study showed that the best results were obtained when ROCK inhibitor was added to the culture medium after seeding single hPSCs on CNT arrays. With ROCK inhibitor treatment, single hPSCs were able to migrate over the CNT arrays surface and reestablish cell–ecell contacts, which was not possible for cultures lacking treatment (Fig. 5). Rho kinases have been shown to have multiple effectors controlling cytoskeleton and cell migration in somatic cells [42–44]. Our study revealed that inhibition of ROCK modifies hPSCs cytoskeleton allowing migration on structured CNT surfaces. Thus, the CNT array surface properties have an effect on hPSC behavior and limit the migration of undifferentiated cells potentially due to their poorly developed cytoskeleton, similar to the case of mouse ESCs [40]. It has also been seen that actin-myosin contractility plays a vital role in monolayer hESC survival [45]. Further studies are needed to unveil the differences in cytoskeletal control of undifferentiated hPSCs and their differentiated progeny. In line with these findings, we found single hPSCs to be highly sensitive to changes in surrounding microenvironment.

3.4. hPSC differentiation on CNTs

To further investigate the influence of CNT arrays on the differentiation capability of hPSCs, we sought to induce spontaneous differentiation in basal medium containing bovine serum without the presence of any additional growth factors and compare it to cells differentiated under identical conditions on TCP as outlined in Fig. 6. In brief, CNT arrays (1×1 cm^2) were UV/ozone treated, disinfected with 70% ethanol, washed with PBS, placed in single wells of 24-well plate, and coated with Geltrex. To exclude the possible supportive role of cytokines produced by differentiating cells on TCP, we transferred CNT arrays with attached cells to new wells. For hESC colonies attached to CNT arrays and hESCs left on plastic in 24-well plates, the medium was replaced with differentiation medium on the following day (Day 0). All cells were immunostained for germ layer-specific markers on Day 16 and 24. Alternatively, EBs were plated onto CNT arrays on Day 8 of suspension culture in differentiation medium and immunostained on Day 16 and Day 24 of differentiation.

There was a noticeable disparity between cells grown on TCP and cells on CNT arrays with minor cell death observed in the middle of CNT arrays. Differentiating cells from both colonies and EBs tended to grow along the perimeter of CNT arrays and migrate on to the TCP. However, cells on CNT arrays were able to differentiate to derivatives of all three embryonic germ layers as was shown by immunocytochemistry and semi-quantitative RT-PCR (Figs. 7–12).

3.4.1. CNT arrays enhance hPSC differentiation—CNT arrays enhanced the differentiation of hPSCs as was evaluated by loss of OCT4 and SOX2 pluripotency markers in comparison with differentiating cells on TCP. Although SOX2 is also an early marker of neural differentiation, its expression was greatly diminished in H9 colonies by Day 16 on CNT arrays (Fig. 7A) and neither OCT4 nor SOX2 were detectable by immunocytochemistry on Day 24 on CNT arrays or TCP (data not shown). Similar results were observed for BM1M iPSC line with Fig. 8A showing the absence of OCT4 and no SOX2 expression in hiPSC colonies on the CNT arrays on Day 16. In contrast, numerous cells expressed pluripotency markers on TCP on matching time points. OCT4 and SOX2 expression was abundant in BM1M hiPSC on TCP even after 24 days in differentiation medium, suggesting general hiPSC line-specific slowed differentiation (Fig. 8B). Enhanced differentiation of hPSC was also observed for EBs on CNT arrays on Day 24 in comparison with cells on TCP (Figs. 10 and 11B).

3.4.2. Embryoid body formation affects hPSC gene and protein expression —After 8 days of EB suspension culture and 8 days of spontaneous differentiation on CNT arrays, hPSCs retained high expression of pluripotency markers at gene and protein levels with down-regulation observed by day 24 (Figs. 9–12). The results of RT-PCR analysis for H9 hESC line in Fig. 12 showed that only EBs after 8 days on CNT arrays (EB D16) expressed all three germ layer markers analyzed in this study. Similar results were observed for EBs on day 24 differentiation on TCP, further suggesting the delayed differentiation capabilities as opposed to cells on CNT arrays (Fig. 12). CNT arrays limited migration of undifferentiated hPSCs, supported the 3D growth of EBs by preventing flattening and spreading and favored the development of vessel-like structures of KDR positive cells and more late endothelial cell marker CD31-positive cells. Fig. 10 shows multiple KDR and CD31 expressing cells in H9 EB on day 24. No CD31 positive progenitors were detected on TCP control samples.

3.4.3. CNT arrays promote germ layer specification—The gene expression profile for H9 hESCs differentiated on CNT arrays showed upregulation of early three germ layer markers (*PAX6* – ectoderm, *KDR* – mesoderm, *AFP* – endoderm and few *SOX17* – late definitive endoderm) and hESCs differentiated on TCP expressed late germ layer markers (*SOX1* – ectoderm, *MIXL1* – mesoderm, *SOX17* – endoderm) (Fig. 12), however immunostaining results clearly demonstrated differences in progenitors generated during spontaneous differentiation. Although *KDR* gene expression was detected in undifferentiated hESCs [46,47] and altered during the differentiation process (Fig. 12), we were able to detect abundant KDR expression through immunocytochemistry only on Day 24 of differentiation in colonies and on Day 16 and 24 in EBs (Figs. 7–11). Differentiation on

CNT arrays leads us to a number of KDR positive (mesoderm, cardiac, hemato-endothelial early progenitor cell marker) progenitors and eliminates the possibility of neural differentiation. hESCs differentiation on TCP lead to an abundant growth of NCAM and *PAX6* positive neural progenitor cells, which are easily distinguishable by characteristic de novo colony-like compact cell clusters with KDR positive cells absent or rare (Figs. 7 and 10). Surprisingly, differentiation of BM1M iPSCs in every culture condition supported growth of almost exclusively KDR positive cells (Figs. 8 and 11), which we hypothesize is the result of the genetic background of the hiPSC line (bone marrow-derived). AFP was also abundantly expressed in differentiating hESCs, however we were not able to detect protein expression through immunocytochemistry.

4. Conclusions

In this study we demonstrated that three key CNT array properties of surface roughness, topography, and stiffness in combination determined the hPSC response and the downstream macroscopic events including survival, migration and differentiation. hPSCs were able to differentiate to all three embryonic germ layers when cultured on CNT arrays. Upon guiding the cells to undergo spontaneous differentiation, in contrast to ECM-coated tissue culture plastic, hPSCs chose the mesodermal lineage in response to the CNT substrate physical characteristics. This study introduces a generation of platforms based on CNT arrays that can be exploited for the identification and modulation of signaling pathways that dictate hPSC response to surrounding biophysical cues. Such a fundamental understanding will help guide strategies aiming at development of biomimetic scaffolds for tissue engineering and regenerative medicine applications.

Acknowledgments

We wish to thank Dr. I. Slukvin and Dr. K. Hu (University of Wisconsin-Madison) for hiPSC lines provided. We also would like to acknowledge Dr. Julia Greer's help with nanoindentation measurements of carbon nanotube arrays. We also would like to acknowledge W. M. Keck Foundation Open Laboratory at USC for the help with AFM measurements. We gratefully acknowledge support from the National Institute of Health (Grant NIH P20 GM103641) and National Science Foundation (Grant EPS-0903795).

References

[1]. Thomson JA, Itskovitz-Eldor J, Shapiro SS, Waknitz MA, Swiergiel JJ, Marshall VS, et al. Embryonic stem cell lines derived from human blastocysts. Science. 1998; 282(5391):1145–7. [PubMed: 9804556]

[2]. Reubinoff BE, Pera MF, Fong CY, Trounson A, Bongso A. Embryonic stem cell lines from human blastocysts: somatic differentiation in vitro. Nat Biotechnol. 2000; 18(4):399–404. [PubMed: 10748519]

[3]. Takahashi K, Tanabe K, Ohnuki M, Narita M, Ichisaka T, Tomoda K, et al. Induction of pluripotent stem cells from adult human fibroblasts by defined factors. Cell. 2007; 131(5):861–72. [PubMed: 18035408]

[4]. Yu JY, Vodyanik MA, Smuga-Otto K, Antosiewicz-Bourget J, Frane JL, Tian S, et al. Induced pluripotent stem cell lines derived from human somatic cells. Science. 2007; 318(5858):1917–20. [PubMed: 18029452]

[5]. Hu KJ, Yu JY, Suknuntha K, Tian SL, Montgomery K, Choi KD, et al. efficient generation of transgene-free induced pluripotent stem cells from normal and neoplastic bone marrow and cord blood mononuclear cells. Blood. 2011; 117(14):E109–19. [PubMed: 21296996]

[6]. Turksen, K. Human embryonic stem cell protocols. Humana Press; Totowa, N.J.: 2006.

[7]. Keung AJ, Healy KE, Kumar S, Schaffer DV. Biophysics and dynamics of natural and engineered stem cell microenvironments. Wires Syst Biol Med. 2010; 2(1):49–64.

[8]. Ma-Moto T, Ingber DE. Mechanical control of tissue and organ development. Development. 2010; 137(9):1407–20. [PubMed: 20388652]

[9]. Chen CS, Mrksich M, Huang S, Whitesides GM, Ingber DE. Geometric control of cell life and death. Science. 1997; 276(5317):1425–8. [PubMed: 9162012]

[10]. Engler AJ, Sen S, Sweeney HL, Discher DE. Matrix elasticity directs stem cell lineage specification. Cell. 2006; 126(4):677–89. [PubMed: 16923388]

[11]. Zoldan J, Karagiannis ED, Lee CY, Anderson DG, Langer R, Levenberg S. The influence of scaffold elasticity on germ layer specification of human embryonic stem cells. Biomaterials. 2011; 32(36):9612–21. [PubMed: 21963156]

[12]. Reilly GC, Engler AJ. Intrinsic extracellular matrix properties regulate stem cell differentiation. J Biomech. 2010; 43(1):55–62. [PubMed: 19800626]

[13]. Gerecht S, Bettinger CJ, Zhang Z, Borenstein JT, Vuniak-Novakovic G, Langer R. The effect of actin disrupting agents on contact guidance of human embryonic stem cells. Biomaterials. 2007; 28(28):4068–77. [PubMed: 17576011]

[14]. Chen A, Lieu DK, Freschauf L, Lew V, Sharma H, Wang JX, et al. Shrink-film configurable multiscale wrinkles for functional alignment of human embryonic stem cells and their cardiac derivatives. Adv Mater. 2011; 23(48):5785–91. [PubMed: 22065428]

[15]. Chen WQ, Villa-Diaz LG, Sun YB, Weng SN, Kim JK, Lam RHW, et al. Nanotopography influences adhesion, spreading, and self-renewal of human embryonic stem cells. ACS Nano. 2012; 6(5):4094–103. [PubMed: 22486594]

[16]. Li XM, Fan YB, Watari F. Current investigations into carbon nanotubes for biomedical application. Biomed Mater. 2010; 5(2):022001.

[17]. Klingeler, R.; Sim, RB. Carbon nanotubes for biomedical applications. Springer; Berlin; New York: 2011.

[18]. Kam NWS, Jessop TC, Wender PA, Dai HJ. Nanotube molecular transporters: internalization of carbon nanotube-protein conjugates into mammalian cells. J Am Chem Soc. 2004; 126(22): 6850–1. [PubMed: 15174838]

[19]. Cui HF, Vashist SK, Al-Rubeaan K, Luong JHT, Sheu FS. Interfacing carbon nanotubes with living mammalian cells and cytotoxicity issues. Chem Res Toxicol. 2010; 23(7):1131–47. [PubMed: 20402485]

[20]. Serag MF, Kaji N, Gaillard C, Okamoto Y, Terasaka K, Jabasini M, et al. Trafficking and subcellular localization of multiwalled carbon nanotubes in plant cells. ACS Nano. 2011; 5(1): 493–9. [PubMed: 21141871]

[21]. Aria AI, Gharib M. Reversible tuning of the wettability of carbon nanotube arrays: the effect of ultraviolet/ozone and vacuum pyrolysis treatments. Langmuir. 2011; 27(14):9005–11. [PubMed: 21671597]

[22]. Seidel GD, Puydupin-Jamin AS. Analysis of clustering, interphase region, and orientation effects on the electrical conductivity of carbon nanotube-polymer nanocomposites via computational micromechanics. Mech Mater. 2011; 43(12):755–74.

[23]. Lonjon A, Demont P, Dantras E, Lacabanne C. Electrical conductivity improvement of aeronautical carbon fiber reinforced polyepoxy composites by insertion of carbon nanotubes. J Non-Cryst Solids. 2012; 358(15):1859–62.

[24]. Sridharan I, Kim T, Wang R. Adapting collagen/CNT matrix in directing hESC differentiation. Biochem Bioph Res Co. 2009; 381(4):508–12.

[25]. Akasaka T, Yokoyama A, Matsuoka M, Hashimoto T, Watari F. Maintenance of hemiround colonies and undifferentiated state of mouse induced pluripotent stem cells on carbon nanotube-coated dishes. Carbon. 2011; 49(7):2287–99.

[26]. Hahm MG, Kwon YK, Busnaina A, Jung YJ. Structure controlled synthesis of vertically aligned carbon nanotubes using thermal chemical vapor deposition process. J Heat Trans-T Asme. 2011; 133(3):031001–5.

[27]. Wiegemann M, Lehmann F. High-throughput SEM preparation of proteinaceaous extracellular matrix. J Mater Sci. 2009; 44(14):3813–8.

[28]. Pryzkhova MV, Harris GM, Shuguo M, Jabbarzadeh E. Patterning pluripotent stem cells at a single cell level. J Biomaterials Tissue Eng. 2013; 3(4):461–71.

[29]. Iijima S. Helical microtubules of graphitic carbon. Nature. 1991; 354(6348):56–8.

[30]. van Kooten TG, Spijker HT, Busscher HJ. Plasma-treated polystyrene surfaces: model surfaces for studying cell-biomaterial interactions. Biomaterials. 2004; 25(10):1735–47. [PubMed: 14738836]

[31]. Ellis SJ, Tanentzapf G. Integrin-mediated adhesion and stem-cell-niche interactions. Cell Tissue Res. 2010; 339(1):121–30. [PubMed: 19588168]

[32]. Braam SR, Zeinstra L, Litjens S, Ward-van Oostwaard D, van den Brink S, van Laake L, et al. Recombinant vitronectin is a functionally defined substrate that supports human embryonic stem cell self-renewal via alpha V beta 5 integrin. Stem Cells. 2008; 26(9):2257–65. [PubMed: 18599809]

[33]. Rowland TJ, Miller LM, Blaschke AJ, Doss EL, Bonham AJ, Hikita ST, et al. Roles of integrins in human induced pluripotent stem cell growth on matrigel and vitronectin. Stem Cells Dev. 2010; 19(8):1231–40. [PubMed: 19811096]

[34]. Ushiki T. Collagen fibers, reticular fibers and elastic fibers. A comprehensive understanding from a morphological viewpoint. Arch Histol Cytol. 2002; 65(2):109–26. [PubMed: 12164335]

[35]. Brunetti V, Maiorano G, Rizzello L, Sorce B, Sabella S, Cingolani R, et al. Neurons sense nanoscale roughness with nanometer sensitivity. Proc Natl Acad Sci USA. 2010; 107(14):6264–9. [PubMed: 20308580]

[36]. Janmey PA, Miller RT. Mechanisms of mechanical signaling in development and disease. J Cell Sci. 2011; 124(1):9–18. [PubMed: 21172819]

[37]. Mih JD, Sharif AS, Liu F, Marinkovic A, Symer MM, Tschumperlin DJ. A multiwell platform for studying stiffness-dependent cell biology. PLoS One. 2011; 6(5):e19929. [PubMed: 21637769]

[38]. Chowdhury F, Li YZ, Poh YC, Yokohama-Tamaki T, Wang N, Tanaka TS. Soft substrates promote homogeneous self-renewal of embryonic stem cells via downregulating cell-matrix tractions. PLoS One. 2010; 5(12):e15655. [PubMed: 21179449]

[39]. Lutolf MP, Hubbell JA. Synthetic biomaterials as instructive extracellular microenvironments for morphogenesis in tissue engineering. Nat Biotechnol. 2005; 23(1):47–55. [PubMed: 15637621]

[40]. Schwartz M. Rho signalling at a glance. J Cell Sci. 2004; 117(23):5457–8. [PubMed: 15509861]

[41]. Agudelo-Garcia PA, De Jesus JK, Williams SP, Nowicki MO, Chiocca EA, Liyanarachchi S, et al. Glioma cell migration on three-dimensional nanofiber scaffolds is regulated by substrate topography and abolished by inhibition of STAT3 signaling. Neoplasia. 2011; 13(9):831–40. [PubMed: 21969816]

[42]. Aspenstrom P. The Rho GTPases have multiple effects on the actin cytoskeleton. Exp Cell Res. 1999; 246(1):20–5. [PubMed: 9882511]

[43]. Begum R, Nur-E-Kamal MSA, Zaman MA. The role of Rho GTPases in the regulation of the rearrangement of actin cytoskeleton and cell movement. Exp Mol Med. 2004; 36(4):358–66. [PubMed: 15365255]

[44]. Hall A, Nobes CD. Rho GTPases: molecular switches that control the organi-zation and dynamics of the actin cytoskeleton. Philos Trans R Soc Lond B Biol Sci. 2000; 355(1399):965–70. [PubMed: 11128990]

[45]. Chen GK, Hou ZG, Gulbranson DR, Thomson JA. Actin-myosin contractility is responsible for the reduced viability of dissociated human embryonic stem cells. Cell Stem Cell. 2010; 7(2):240–8. [PubMed: 20682449]

[46]. Yang L, Soonpaa MH, Adler ED, Roepke TK, Kattman SJ, Kennedy M, et al. Human cardiovascular progenitor cells develop from a KDR plus embryonicstem-cell-derived population. Nature. 2008; 453(7194):524–8. [PubMed: 18432194]

[47]. Vodyanik MA, Bork JA, Thomson JA, Slukvin II. Human embryonic stem cell-derived CD34(+) cells: efficient production in the coculture with OP9 stromal cells and analysis of lymphohematopoietic potential. Blood. 2005; 105(2):617–26. [PubMed: 15374881]

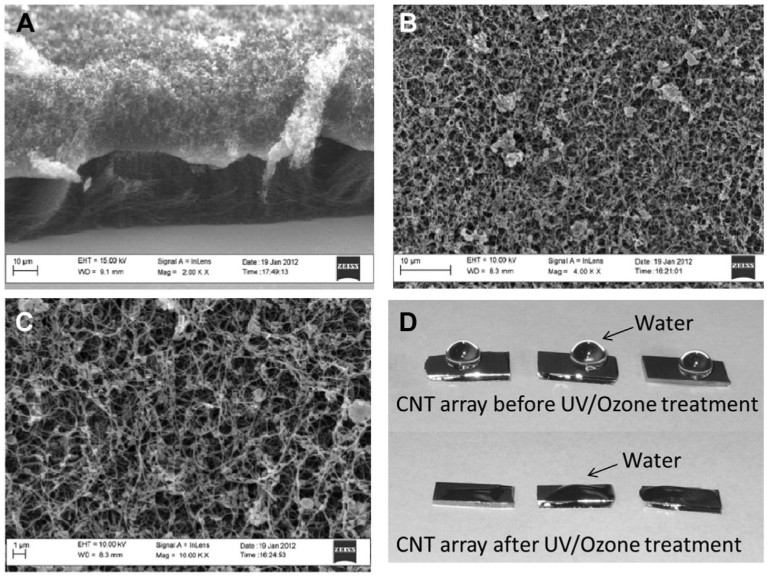

Fig. 1.

SEM images of CNT arrays on silicon wafer. (A) Entire array structure from side view. (B, C) Incorporation of ECM proteins (Geltrex) onto the surface of UV/ozone treated CNT arrays (magnification 4000 and 10,000 correspondingly). (D) Hydrophobic CNT arrays on the silicon wafers before UV/ozone treatment and the same CNT arrays became hydrophilic after oxidation as seen with water drop assay.

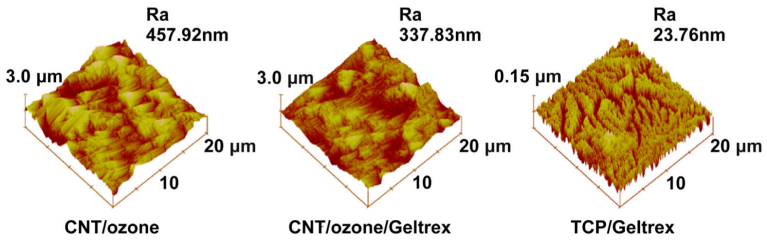

Fig. 2.

AFM analysis of surface roughness. Representative images of cell culture surface topography: CNT – carbon nanotubes, TCP – tissue culture plastic, Ra – the average deviation from mean.

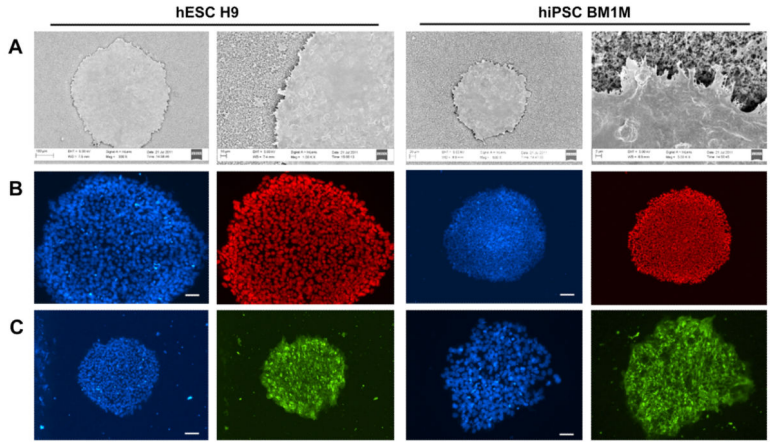

Fig. 3.

hPSC colonies grown on CNT arrays demonstrate typical morphology and express pluripotency-associated markers characteristic for undifferentiated cells. (A) SEM images of hPSC colonies on CNT array (magnification 300, 1000, 500 and 5000). (B) Expression of transcription factor OCT4 (red) in hPSC colonies (scale bar 50 μm and 100 mm). (C) Expression of trans-membrane protein TRA-1-81 (green) (scale bar 100 μm and 50 μm correspondingly). Cell nuclei are stained with DAPI (blue). (For interpretation of the references to color in this figure legend, the reader is referred to the web version of this article.)

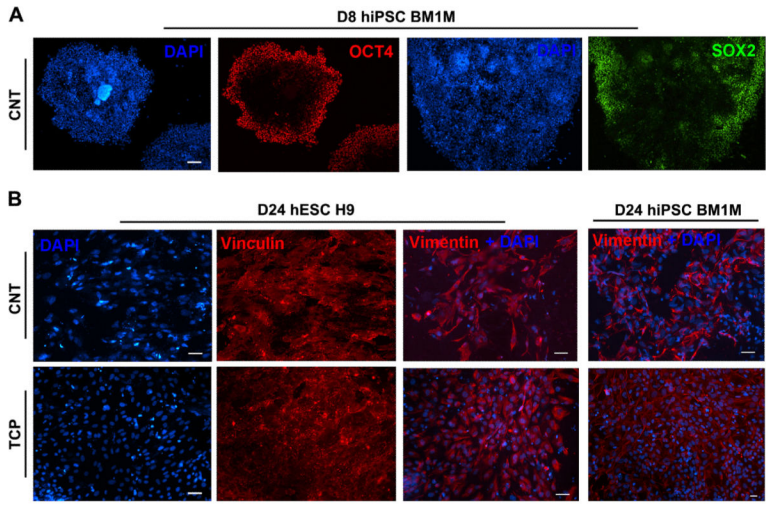

Fig. 4.

Behavior of hPSCs on CNT arrays. (A) hPSCs lose pluripotency marker expression in the middle of colonies first (Day 8 of differentiation) (scale bar 100 μm). (B) By Day 24 of differentiation cells lose cell–cell contacts, migrate out of colonies, and demonstrate multiple focal adhesion sites (scale bar 50 μm).

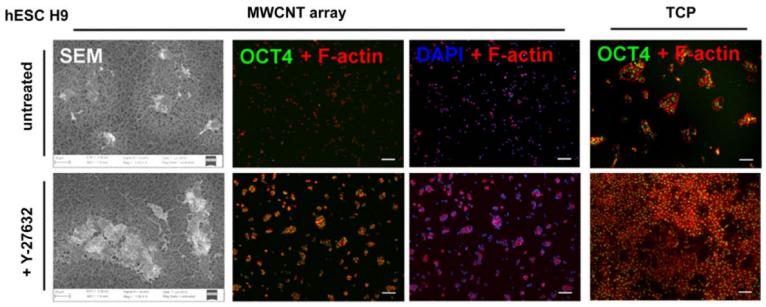

Fig. 5.

hPSC from a monolayer culture seeded on CNT arrays as a homogenous single cell suspension, in contrast to cells on TCP, underwent apoptosis within 24 h if ROCK inhibitor (Y-27632) was not added. However the addition of 10 μm ROCK inhibitor allowed single hPSCs to migrate on CNT arrays and reestablish cell–cell contacts similar to cells on TCP.

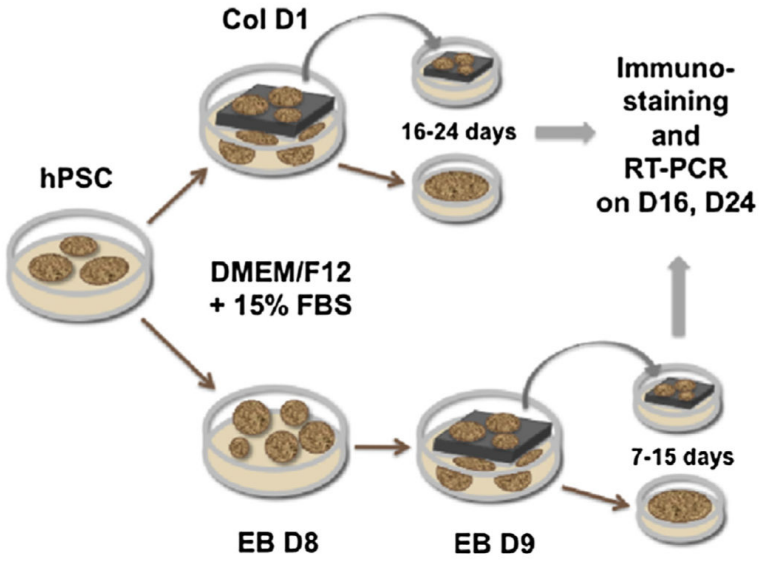

Fig. 6.
Schematic of hPSC differentiation process in colonies (Col) and embryoid bodies (EB).

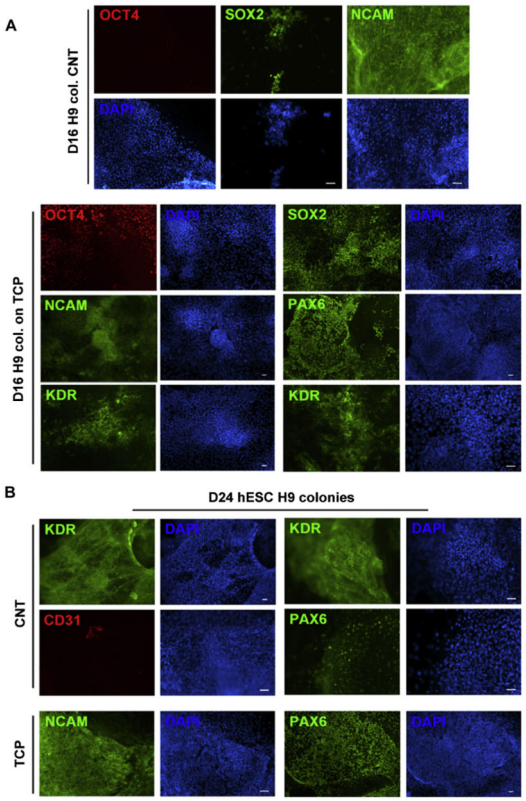

Fig. 7.

Spontaneous differentiation of hESC H9 colonies on CNT arrays and tissue culture plastic analyzed on Day 16 (A) and 24 (B) (scale bar 50 μm).

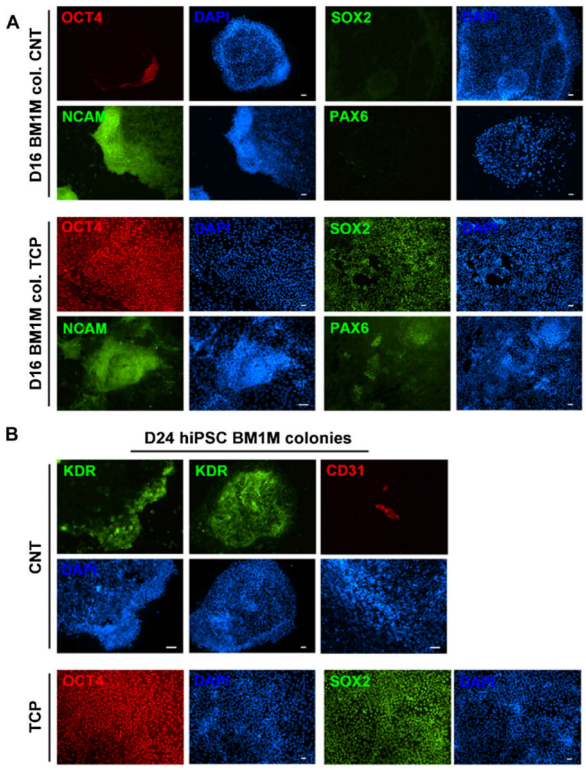

Fig. 8.

Spontaneous differentiation of hiPSC BM1M colonies on CNT arrays and tissue culture plastic analyzed on Day 16 (A) and 24 (B) (scale bar 50 μm).

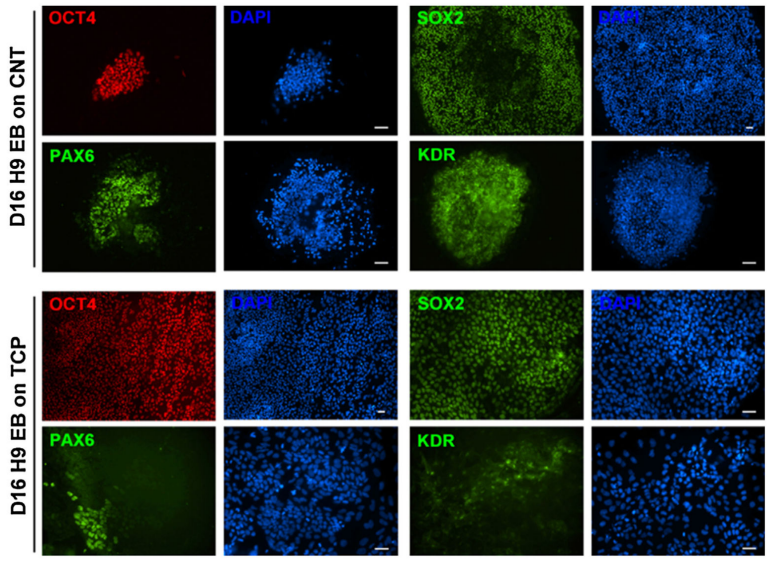

Fig. 9.

Spontaneous differentiation of hESC H9 embryoid bodies on CNT arrays and tissue culture plastic analyzed on Day 16 (scale bar 50 μm).

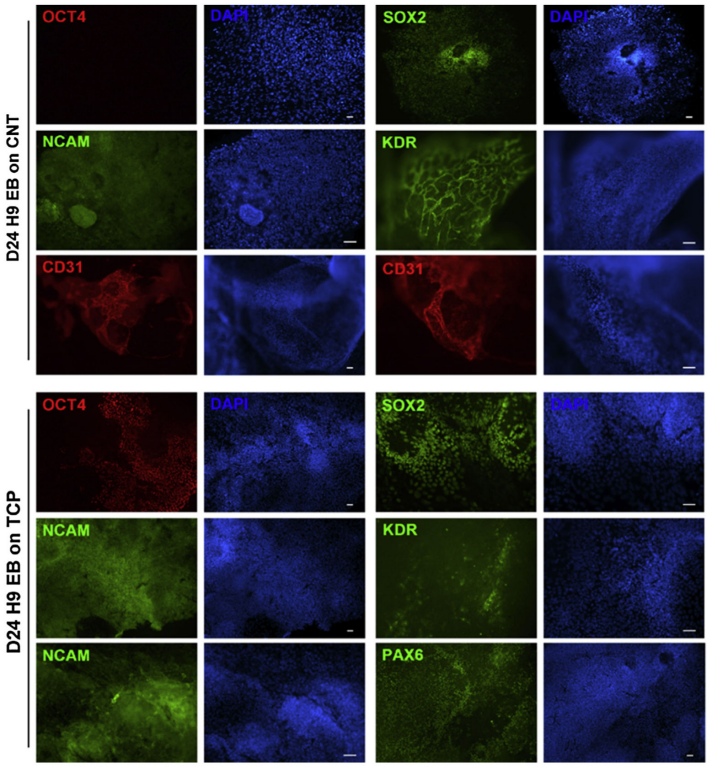

Fig. 10.

Spontaneous differentiation of hESC H9 embryoid bodies on CNT arrays and tissue culture plastic analyzed on Day 24 (scale bar 50 μm).

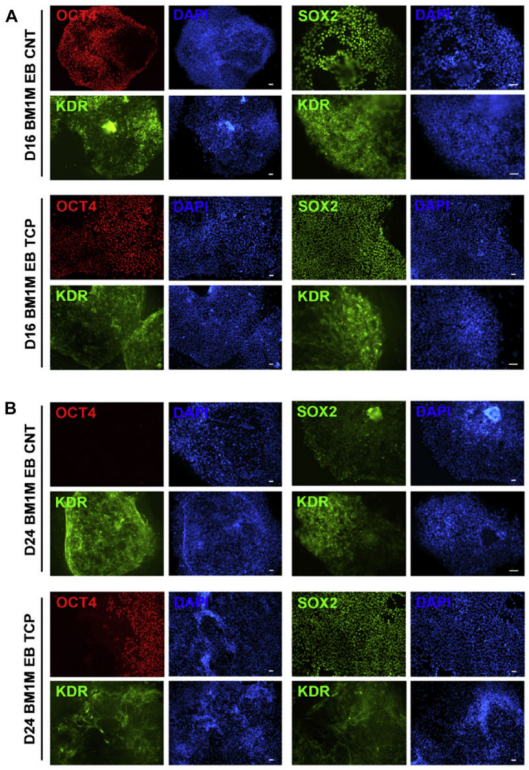

Fig. 11.

Spontaneous differentiation of hiPSC BM1M embryoid bodies on CNT arrays and tissue culture plastic analyzed on Day 16 (A) and Day 24 (B) (scale bar 50 μm).

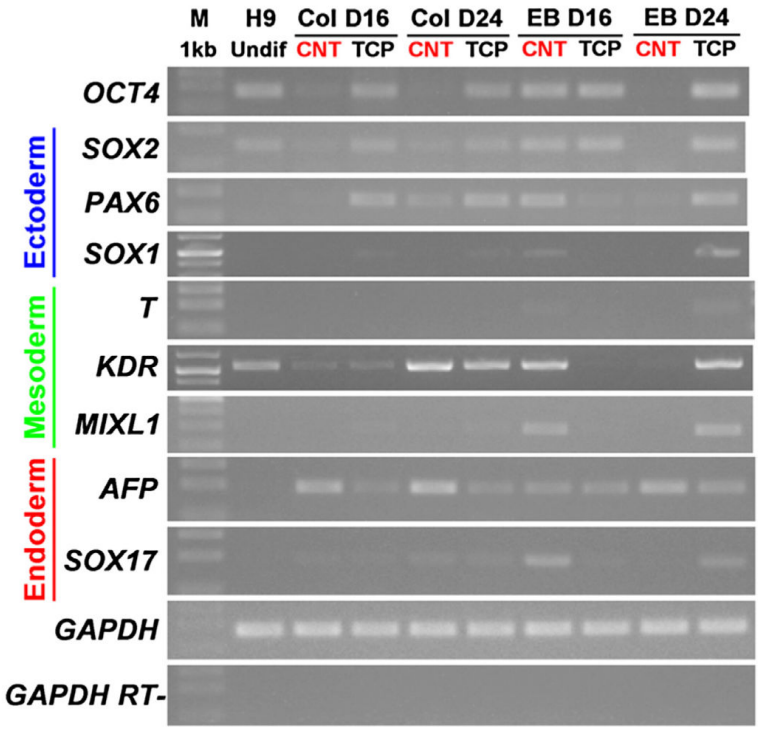

Fig. 12.

RT-PCR analysis of gene expression of undifferentiated H9 hESC and Day 16 and Day 24 cells differentiated on CNT arrays and TCP from colonies and embryoid bodies.

Table 1

Antibodies.

Antibodies	Isotype	Catalog#	Provider
Primary antibodies			
Anti-OCT3/4 (C-10)	Mouse IgG_{2b}	sc-5279	Santa Cruz
Anti-TRA-1-81 (TRA-1-80)	Mouse IgM	sc-21706	Santa Cruz
Anti-SOX2	Rabbit IgG	09-0024	Stemgent
Anti-CD56/NCAM (EP2567Y)	Rabbit IgG	2433-1	Epitomics
Anti-PAX6	Rabbit IgG	09-0075	Stemgent
Anti-BRA (D-10)	Mouse IgM	sc-166962	Santa Cruz
Anti-VEGFR2/KDR (55B11)	Rabbit IgG	2479S	Cell Signaling
Anti-CD31/PECAM-1 (89C2)	Mouse IgG_{2b}	3528	Cell Signaling
Anti-AFP (3H8)	Mouse IgG_{2a}	3903S	Cell Signaling
Anti-vimentin (V9)	Mouse IgG_1	sc-6260	Santa Cruz
Anti-vinculin (hVIN-1)	Mouse IgG_1	V9264	Sigma
Secondary antibodies			
Anti-mouse Alexa Fluor 488	Goat IgG	A31620	Invitrogen
Anti-mouse Alexa Fluor 488	Goat IgM	A21042	Invitrogen
Anti-rabbit Alexa Fluor 488	Goat IgG	A31628	Invitrogen
Anti-mouse Alexa Fluor 594	Goat IgG	A31624	Invitrogen

Table 2

PCR primers.

Gene	5′–3′ primer sequences: (F: forward, R: reverse)	Product size, bp
OCT4	F: CAGTGCCCGAAACCCACAC R: GGAGACCCAGCAGCCTCAAA	161
SOX2	F: TACCTCTTCCTCCCACTCCA R: GGTAGTGCTGGGACATGTGA	131
SOX1	F: CAATGCGGGGAGGAGAAGTC R: CTCTGGACCAAACTGTGGCG	464
PAX6	F: TGTCCAACGGATGTGTGAGT R: TTTCCCAAGCAAAGATGGAC	162
BRA	F: ACCCAGTTCATAGCGGTGAC R: CCATTGGGAGTACCCAGGTT	165
KDR	F: ATGCACGGCATCTGGGAATC R: GCTACTGTCCTGCAAGTTGCTGTC	573
MIXL1	F: ACGTCTTTCAGCGCCGAACAG R: TTGGTTCGGGCAGGCAGTTCA	292
AFP	F: AGCTTGGTGGTGGATGAAAC R: TCTGCAATGACAGCCTCAAG	182
SOX17	F: CGCACGGAATTTGAACAGTA R: GGATCAGGGACCTGTCACAC	182
GAPDH	F: GTGGACCTGACCTGCCGTCT R: GGAGGAGTGGGTGTCGCTGT	153

Table 3

AFM analysis of cell culture surface roughness, calculated on 20 × 20 μm^2 regions.

Substrate	Ra[a] (nm)	Rq[b] (nm)
Tissue culture treated polystyrene (TCP)	4.22	5.74
Geltrex-coated TCP	23.76	28.11
CNT array	494.23	636.10
UV/ozone treated CNT array	457.92	555.13
Geltrex-coated, UV/ozone treated CNT array	337.83	428.07

[a]The average deviation from mean.

[b]The root-mean-square deviation.